

ViViDex: Learning Vision-based Dexterous Manipulation from Human Videos

Zerui Chen¹, Shizhe Chen¹, Cordelia Schmid¹ and Ivan Laptev²

Abstract—In this work, we aim to learn a unified vision-based policy for a multi-fingered robot hand to manipulate different objects in diverse poses. Though prior work has demonstrated that human videos can benefit policy learning, performance improvement has been limited by physically implausible trajectories extracted from videos. Moreover, reliance on privileged object information such as ground-truth object states further limits the applicability in realistic scenarios. To address these limitations, we propose a new framework ViViDex to improve vision-based policy learning from human videos. It first uses reinforcement learning with trajectory guided rewards to train state-based policies for each video, obtaining both visually natural and physically plausible trajectories from the video. We then rollout successful episodes from state-based policies and train a unified visual policy without using any privileged information. A coordinate transformation method is proposed to significantly boost the performance. We evaluate our method on three dexterous manipulation tasks and demonstrate a large improvement over state-of-the-art algorithms. The project page is available at <https://zerchen.github.io/projects/vividex.html>.

I. INTRODUCTION

Humans possess a remarkable ability to manipulate diverse objects using their hands based on visual perception. Nevertheless, compared with parallel grippers [1], [2], [3], [4], [5], [6], achieving comparable levels of dexterous manipulation with multi-fingered robot hands remains an ongoing challenge [7]. It requires to convert visual signals to high-dimensional control commands.

In recent years, the advancement of deep learning (DL) [8] and reinforcement learning (RL) [9], [10] has led to significant progress in learning-based algorithms for dexterous manipulation such as in-hand rotation [11], [12], [13], solving Rubik’s cube [14] and playing the piano like humans [15], [16]. However, it proves challenging to train RL policies as RL training heavily relies on intricate reward engineering [10], [17] and extensive computational resources [14]. Furthermore, unnatural behaviors with high rewards can emerge from RL training [18]. To address the limitations of RL training, some previous works [19], [20], [21], [22] have turned to imitation learning using robot demonstrations collected by teleoperation. While these approaches enhance training efficiency, they demand substantial human efforts to collect diverse robot demonstration data and are, hence, difficult to scale.

As human videos capturing hands manipulating objects are more abundant and easy to acquire, an increasing research

attention has been paid to leveraging human videos for learning dexterous manipulation skills [23], [24], [25], [26], [27]. For example, DexMV [23] proposes to automatically extract robot and object poses from human videos, and then employs the data to accelerate RL via demonstration augmented policy gradient (DAPG) [19]. However, since the extracted robot and object poses are noisy, the method needs hundreds of human videos to learn the manipulation of a single object and still requires reward engineering for different tasks. Additionally, existing works [23], [25], [28] take advantage of privileged information of objects in policy learning such as known object CAD models and ground-truth object poses, which are non-trivial to obtain from raw visual sensors in real-world scenarios.

In this work, we propose a new framework called ViViDex to leverage human Videos for Vision-based Dexterous Manipulation policy learning. It consists of three modules as illustrated in Figure 1: reference trajectory extraction, trajectory guided state-based policy learning, and unified vision-based policy learning. We first obtain reference trajectories for hands and objects from human videos following prior work [23]. Though such trajectories are noisy and not directly suitable for robot control, they provide examples of natural hand-object interactions that we use as guidance. Our second module refines and recovers physics properties of the reference trajectory. We use RL for this purpose by training a state-based policy for each reference trajectory. We design a novel reward to keep pose similarity in the reference trajectory while solving the task. We also augment the trajectory during training to generalize to a broader range of object poses beyond the pose in the reference trajectory. Finally, we rollout episodes from optimized state-based policies and distill successful episodes to a unified vision-based policy without any privileged object information. A coordinate transformation method is proposed to improve the vision-based policy, which transforms the input 3D point clouds into hand joints and the target coordinate systems to capture fine-grained interaction features and increase awareness of the target position. We validate the effectiveness of our system on three dexterous manipulation tasks *relocation*, *pouring* and *placing inside*. Our ViViDex approach significantly outperforms the state-of-the-art method DexMV [23] while using significantly less human demonstrations.

To summarize, our contributions are three-fold:

- We introduce a new framework ViViDex to learn vision-based dexterous manipulation policy from human videos.
- We improve the RL rewards for the state-based policy

¹Inria, École normale supérieure, CNRS, PSL Research University, 75005, Paris, France. {firstname.lastname}@inria.fr

²Mohamed bin Zayed University of Artificial Intelligence, Abu Dhabi, United Arab Emirates. {firstname.lastname}@mbzuai.ac.ae

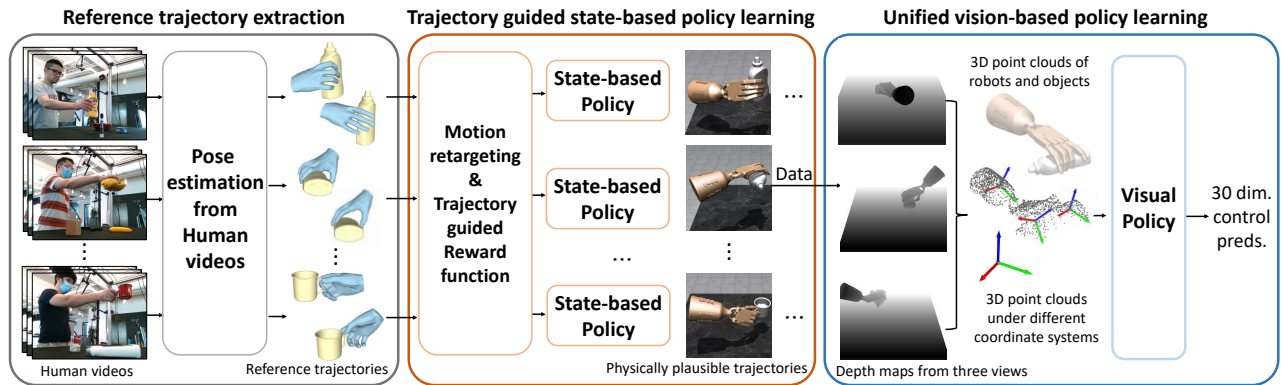


Fig. 1: The overall framework of our method for learning dexterous manipulation skills from human videos. It consists of three modules: the extraction of the reference trajectory from human videos, the trajectory-guided state-based policy learning using RL, and the vision-based policy learning using behavior cloning.

by imitating trajectories extracted from human videos and propose a novel model architecture for the vision-based policy.

- Experiments on three dexterous manipulation tasks demonstrate the effectiveness of the ViViDex approach.

II. RELATED WORK

Dexterous manipulation. The multi-fingered robotic hands empower robots to perform delicate operations on objects like humans. Previous works can be generally grouped into two categories: trajectory optimization methods [29], [30], [31], [32], [33] and data-driven learning methods [19], [23], [24], [28], [34], [35], [36], [37]. Trajectory optimization methods usually require well-defined dynamic models for the robot and the manipulated object, which are usually not easy to obtain in practice. Data-driven methods instead train neural network policies for manipulation, allowing to learn generalizable skills. Most of the works [19], [28], [35], [38], [39], [40] use reinforcement learning (RL) algorithms to train policies. Nagabandi *et al.* [39] and Hansen *et al.* [40] propose to improve the sample efficiency in RL by jointly learning the dynamic model and the control policy. To accelerate the convergence of RL, Rajeswaran *et al.* [19] introduce the demo augmented policy gradient algorithm (DAPG) and train RL with expert demonstrations. Instead of manually collecting expert demonstrations, ILAD [28] derives demonstration data via an affordance model [41] and trajectory optimization [42]. Xu *et al.* [35] and Wan *et al.* [38] decompose the dexterous grasping into two sub-tasks: the grasp proposal generation and the goal-conditioned policy training and largely improve the generalization of the learned policy. However, RL is data-inefficient and requires well-designed rewards, which often results in unrealistic object manipulation actions. To address these problems, more recent works [23], [25], [26], [27] attempt to learn policies using human demonstrations and combine imitation learning with RL.

Learning robotic manipulation from human videos. Human videos naturally provide rich human hands interactions with diverse objects [43], [44], [45], [46], [47]. Equipping robots with the capacity to acquire manipulation skills by simply watching human videos has been an attractive

direction [48], [49], [50], [51], [52]. Some works [34], [53], [54], [55] propose to use human videos to pre-train a visual representation for the policy learning. R3M [34] proposes to pre-train CNNs with egocentric human videos [56] and perform the imitation learning based on the learned visual representations. Xiao *et al.* [53] and Radosavovic *et al.* [54] propose to leverage in-the-wild human videos to pre-train the vision transformer and demonstrate the improvement on different manipulation tasks. The recent work H-InDex [55] employs 3D human pose estimation from human videos as a proxy task to pre-train the visual representation for dexterous manipulation tasks. Another line of works [57], [58], [59], [60] focus on learning the reward function from human videos. Chen *et al.* [57] introduce DVD, a domain-agnostic video discriminator, to learn multi-task reward functions. Alakuijala *et al.* [58] propose a task-agnostic reward function by using unlabeled human videos. Chane-Sane *et al.* [59] formulate the reward learning as a retrieval task and propose a data-driven approach to map human demonstrations to unseen robotic manipulation tasks. Xiong *et al.* [60] propose to translate human demonstration videos into robot demonstration videos and use the keypoint-based representation to define the distance metric for the policy execution. Some other works [23], [24], [25], [26], [61] explore how to explicitly leverage human videos to facilitate learning dexterous manipulation skills. Mandikal *et al.* [61], [24] propose to utilize object affordances priors and human grasping priors to improve the dexterous grasping policy. Shaw *et al.* [26] propose to first pre-train the policy with visual, action and physical priors learned from human videos and finetune the policy with teleoperated demonstrations to make it generalize to different robotic tasks. DexMV [23] and DexRepNet [25] extract demonstrations data from human videos and uses DAPG algorithm [19] to launch the RL training with demonstrations. In this work, not limited to the simple dexterous grasping action [24], [25], [35], [38], [61], we aim to solve more complex tasks by utilizing human videos. To additionally address limitations of previous works [23], [25], [28] that require object states (*e.g.*, object poses) during the policy execution, we propose learning

TABLE I: The state definition. The left part summarizes robot states. The right part defines object states.

Parameters	Descriptions	Parameters	Descriptions
$\mathbf{q}_r \in \mathbb{R}^{30}$	robot motor positions	$\mathbf{q}_o \in \mathbb{R}^6$	object canonical positions
$\dot{\mathbf{q}}_r \in \mathbb{R}^{30}$	robot motor velocities	$\dot{\mathbf{q}}_o \in \mathbb{R}^6$	object canonical velocities
$\mathbf{x}_r \in \mathbb{R}^{16 \times 3}$	robot joint positions	$\mathbf{x}_o \in \mathbb{R}^3$	object center position
$\boldsymbol{\theta}_r \in \mathbb{R}^{16 \times 4}$	robot joint rotations	$\boldsymbol{\theta}_o \in \mathbb{R}^4$	object global rotation
$\dot{\mathbf{x}}_r \in \mathbb{R}^{16 \times 3}$	robot linear velocities	$\dot{\mathbf{x}}_o \in \mathbb{R}^3$	object linear velocity
$\boldsymbol{\omega}_r \in \mathbb{R}^{16 \times 3}$	robot angular velocities	$\boldsymbol{\omega}_o \in \mathbb{R}^3$	object angular velocity
$\mathbf{t}_r \in \mathbb{R}^{7 \times 3}$	robot target translations	$\mathbf{t}_o \in \mathbb{R}^3$	object target translations

vision-based policies that achieve high manipulation accuracy while only using proprioceptive robot information and depth observations in the form of point clouds.

III. METHOD

This work aims to train vision-based dexterous manipulation policies. However, jointly learning the visual representation and the control policy is challenging. Therefore, we first train the state-based policy and then distill the generated data to a vision-based policy. To train the state-based policy, as the pure RL training is ineffective [23], [25], [28], we extract reference trajectories from human videos and propose trajectory-guided RL to improve the performance. In the following, we first present details about the reference trajectory generation in Section III-A. Then, we introduce our state-based policy learning algorithm in Section III-B. Finally, we describe how we distill multiple state-based policies into the visual policy and its model architecture in Section III-C.

A. Reference Trajectory Extraction

In this work, we use the DexYCB [43] video dataset, which captures human hand grasping of objects. We first extract hand and object poses from the video. The hand poses and shapes are represented by MANO [62] and result in 3D locations of joints $\boldsymbol{\psi}_h \in \mathbb{R}^{21 \times 3}$. Then, we aim to retarget the human hand pose to the robot hand pose. We use the Adroit anthropomorphic robot [19], which consists of 30 degrees of freedom $\mathbf{q}_r \in \mathbb{R}^{30}$. Following [23], [63], [64], we formulate the hand motion retargeting from a video of length T as an optimization problem and define its objective function as:

$$\min_{\mathbf{q}_r^t} \sum_{t=1}^T \left\| \hat{\mathbf{x}}_{rt}^t(\mathbf{q}_r^t) - \boldsymbol{\psi}_{ht}^t \right\|_2^2 + \left\| \hat{\mathbf{x}}_{rp}^t(\mathbf{q}_r^t) - \boldsymbol{\psi}_{hp}^t \right\|_2^2 + \alpha \left\| \mathbf{q}_r^t - \mathbf{q}_r^{t-1} \right\|_2^2, \quad (1)$$

where $\boldsymbol{\psi}_{ht}^t \in \mathbb{R}^{5 \times 3}$ and $\boldsymbol{\psi}_{hp}^t \in \mathbb{R}^{5 \times 3}$ denote human hand tip and middle phalanx positions, respectively. We solve their counterparts $\hat{\mathbf{x}}_{rt}^t$ and $\hat{\mathbf{x}}_{rp}^t$ in the robot via forward kinematics according to given \mathbf{q}_r^t . In the first two terms, we aim to minimize the difference between the 3D locations of robot joints to those in the human hand. We also use a regularization term to avoid sudden changes in the robot pose, where we empirically set α and \mathbf{q}_r^0 to 4e-3 and the mean pose of its motion limits, respectively. We use the NLOpt solver [65] for the optimization and port robot and object motions into the

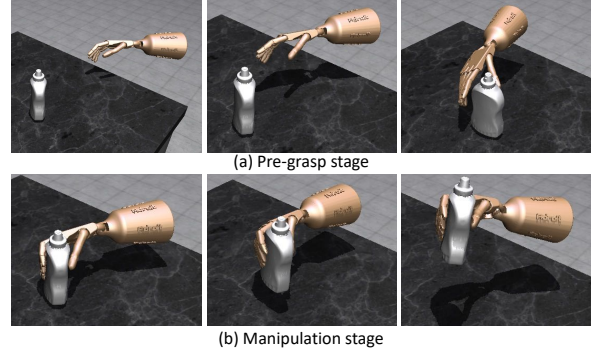


Fig. 2: The illustration of different stages for the reference trajectory. The pre-grasp stage (a) describes how the robot approaches the object. The manipulation stage (b) focuses on how the robot hand manipulates the object.

simulator to generate reference trajectories, which are only visually plausible but not physically plausible.

B. State-based Policy

We employ the generated reference trajectory as the reward function for RL to constrain the robot hand and object motions and train a state-based policy to recover physically plausible trajectories. The network architecture for the state-based policy consists of actor and critic MLPs [66]. It takes both robot and object states described in Table I as inputs and predicts the robot control commands. Different from DexMV [23] that needs different reward functions for different manipulation tasks, our method can solve different tasks with the same reward functions. In the following, we will describe our reward functions and the trajectory augmentation for RL.

Reward functions. To define the reward function, we divide the reference trajectory into two stages shown in Figure 2: the pre-grasp stage and the manipulation stage. The recent work PGDM [27] focuses on the manipulation stage and initializes the robot hand at a given pre-grasp configuration for RL, which is a simplified setting compared with ours.

During the pre-grasp stage, the robot hand approaches the object without making physical contacts. During RL training, we require that the robot approaches the object in a similar way as humans and define the following reward function:

$$R_p = \sum_{t=1}^{T_p} 10 \cdot \exp(-10 \cdot \left\| \mathbf{x}_{rt}^t(\mathbf{q}_r^t) - \hat{\mathbf{x}}_{rt}^t \right\|_2^2), \quad (2)$$

where T_p is the length of pre-grasp steps, and $\hat{\mathbf{x}}_{rt}^t \in \mathbb{R}^{5 \times 3}$ denotes the robot finger tip positions at the timestep t in the reference trajectory \mathbf{x}_{rt}^t is the current robot tip locations.

When the robot successfully reaches its pre-grasp configuration, the episode starts its manipulation stage. In this stage, the robot manipulates the object and aims to bring it to the desired target configuration. Here, we define the reward

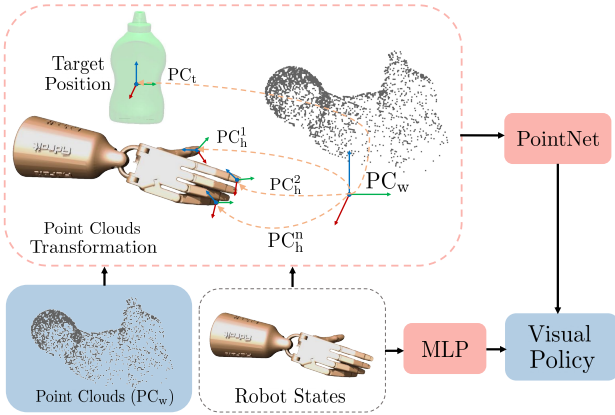


Fig. 3: Illustration of our vision-based policy architecture. function to constrain the robot and object motions jointly:

$$\begin{aligned}
 R_m = & \sum_{t=T_p+1}^{T_r} \lambda_1 \cdot \exp(-\alpha_1 \cdot \|\mathbf{x}_{rt}^t(\mathbf{q}_r^t) - \hat{\mathbf{x}}_{rt}^t\|_2^2) \\
 & + \lambda_2 \cdot \exp(-\alpha_2 \cdot (\|\mathbf{x}_o^t - \hat{\mathbf{x}}_o^t\|_2^2 + \alpha_3 \cdot \phi(\boldsymbol{\theta}_o^t, \hat{\boldsymbol{\theta}}_o^t))) \quad (3) \\
 & + \sum_{i=1}^5 \lambda_3 \cdot \mathbb{1}_{\text{finger } i}^{\text{contact}} + \lambda_4 \cdot \mathbb{1}_{\text{object}}^{\text{lift}},
 \end{aligned}$$

where T_r refers to the length of the whole reference trajectory. The first term of (3) constrains the hand motions similar to (2). The second term constrains the object motions, and \mathbf{x}_o^t and $\hat{\mathbf{x}}_o^t$ represent the current object position and the reference object position at timestep t . $\phi(\cdot)$ computes the angular distance between the current object orientation with its reference $\hat{\boldsymbol{\theta}}_o^t$. In the third term, we encourage contacts between each finger of the robot and the object. The fourth term assigns bonus points when the object is lifted off the table. The second and fourth terms are introduced in [27], and we use the same hyperparameters (*i.e.*, $\lambda_2 = 10$, $\alpha_2 = 50$, $\alpha_3 = 0.1$ and $\lambda_4 = 2.5$). For our proposed first and third terms, we empirically set λ_1 , α_1 and λ_3 to 4, 10 and 0.5, respectively.

When the robot and object reaches their targets, we want them to remain stable in their target configurations for a while, which is especially important for the pour task to make sure that all particles in the mug have enough time to drop into the target container. To achieve this when $t > T_r$, we still use (3) and constrain the robot and object to stay in their final target configurations until the end of the episode.

Reference trajectory augmentation. By using our proposed reward functions, though the state-based policy can successfully imitate the hand and object motions from a video, it still cannot generalize to different initial object positions, rotations and target positions. To make our policy applicable to different initial object configurations and target positions, we introduce our reference trajectory augmentation strategies during RL training. To deal with different initial object positions or rotations, we could accordingly transform the whole reference trajectory. When we randomly set the target object position, we augment the original object trajectory through interpolations aimed at reaching the specified target position. For *pour* and *place inside* tasks, we first design

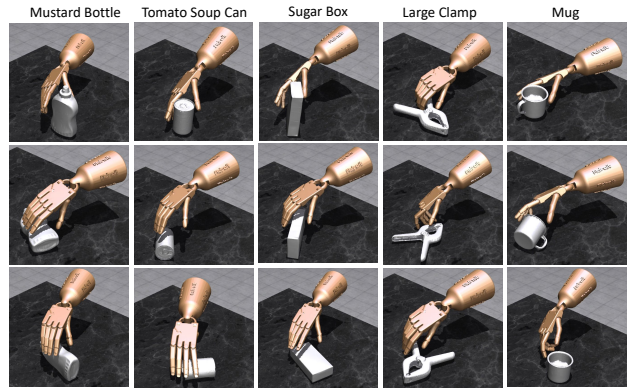


Fig. 4: Motion retargeting results for selected DexYCB [43] videos. The three rows show different initial object poses for each object category.

the desired final object configuration. In the *pour* task, we ensure that the mug is tilted appropriately, which allows the particles inside to effortlessly drop into the target container. Our goal for *place inside* is to accurately position the banana within the container. Then, we interpolate the object position and orientation to reach the desired configuration. Similarly, we can also interpolate hand motions and use our proposed reward functions to optimize the policy.

C. The Vision-based Policy

Though our state-based policy can work well for different manipulation tasks, it requires robot proprioceptive states and object states as inputs. However, reliably estimating object states is often not trivial in practice. To alleviate this issue, we propose a vision-based policy that only takes robot states and 3D scene point clouds as inputs. To generate training data for the visual policy, we rollout the optimized state-based policy and generate diverse physically plausible trajectories. During the rollout process, we compute the 3D point clouds $PC_w \in \mathbb{R}^{N \times 3}$ from three depth cameras in the simulator, where PC_w is represented under the world coordinate system (*i.e.*, the center of the table) and N is the number of points.

As shown in Figure 3, inspired by [5], we propose to transform PC_w into the desired target coordinate system PC_t , which make the model more aware of the target position for control predictions. To capture dense interaction features between the robot and the object, we additionally transform PC_w into six different robot joint coordinate systems (*i.e.*, one wrist and five fingers). Finally, we combine point clouds representations under different coordinate systems $PC \in \mathbb{R}^{N \times 24}$ and feed them into PointNet [67]. Our visual policy predicts control commands based on extracted visual features and robot states. We train our visual policy using behavior cloning from generated physically plausible trajectories.

IV. EXPERIMENTS

We conduct extensive experiments to evaluate our state-based and visual policies on three manipulation tasks, namely *relocate*, *pour* and *place inside* tasks.

TABLE II: Performance of our state-based policy using hand rewards at different stages. It follows the human hand trajectory extracted from videos to manipulate objects (R1), reach the pre-grasp configurations (R2) or combine both (R3).

	Hand Reward		$E_o \downarrow$	$E_h \downarrow$	$SR_o \uparrow$	$SR_h \uparrow$	$SR_3 \uparrow$
	Pre-grasp	Manipulation					
R1	×	✓	0.063	0.15	0.37	0.00	0.00
R2	✓	×	0.0031	0.053	0.93	0.32	1.00
R3	✓	✓	0.0031	0.024	0.95	0.83	1.00

A. Experimental Setting

Video dataset. The DexYCB [43] dataset contains human demonstration videos of hand-object interactions for 20 YCB objects with 20 videos per object. Following [23], we focus on five objects including *mustard bottle*, *tomato soup can*, *sugar box*, *large clamp* and *mug*. Due to the unavailability of DexMV videos [23], we select videos from the DexYCB dataset that shares high visual similarities with DexMV videos. For each object, we choose one video which is most similar to those used in DexMV and use this video for most of our experiments; the top row in Figure 4 presents motion retargeting results for these videos. For the final experiment, we add additional initial configurations of the objects to the test set (different from [23]) and use two additional videos per object with different initial object positions for training, as illustrated in the last two rows of Figure 4. We use hand and object poses provided by the dataset to perform motion retargeting and generate reference trajectories.

Simulation benchmark. We follow previous work [23], [27] and use the MuJoCo physics simulator [68] together with the Adroit robot hand [19]. The robot hand consists of 30 degrees of freedom (DoF). We set the control frequency and simulation frequency as 40HZ and 400HZ, respectively. As discussed above, we use the same testing configuration as in [23] except for the final experiment, where we use a more difficult setting, and evaluate the performance of our method on three manipulation tasks:

Relocate task requires the robot to move an object to a target position. The task is successfully solved when the object reaches the target position within a certain threshold.

Pour task requires the robot to grasp a mug filled with particles and pour the particles into a container. The success rate is measured by the percentage of particles in the container.

Place inside task requires the robot to grasp a banana and place it into a mug. The success rate is measured by the percentage of the banana mesh in the mug.

Evaluation metrics. The success rate (SR) is the major metric for the above three tasks. For the *relocate* task, we adopt the 10cm threshold (SR_{10}) following [23], [28] to define the success rate. To measure the accuracy more precisely, we add a more rigorous threshold of 3cm and compute the success rate SR_3 . For the state-based policy, we additionally evaluate how well the learned physically plausible trajectory matches the reference trajectory in the video using four metrics [27]: E_o computes the average object position error between the current object trajectory and its reference trajectory over time;

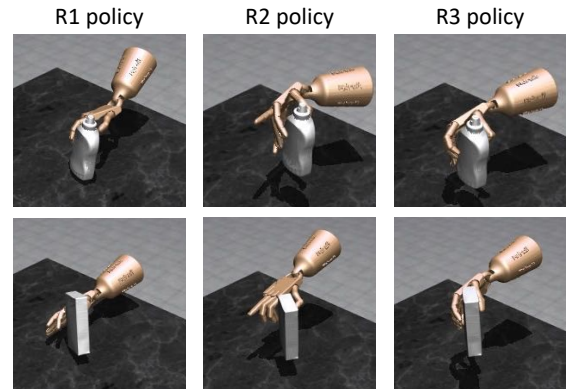


Fig. 5: Qualitative comparison of state-based policies using different rewards. R1 (w/o hand reward in pre-grasp) leads to unstable grasps. R2 (w/o hand reward in manipulation) results in unnatural hand actions. Our proposed policy R3 uses hand rewards at both stages and achieves the best performance.

E_h computes the average finger tips position error between the current robot hand trajectory and its reference trajectory over time; SR_o reports the fraction of timesteps where E_o is below the 1cm threshold; SR_h computes the fraction of timesteps where E_h is lower than 5cm.

Implementation details. During RL training, we randomly set the object initial and target positions following [23] and also randomize the initial object orientation. During testing, we run 300 episodes with different initial configurations and report the average success rate. For the state-based policy, we use both robot and object states defined in Table I as inputs and predict the control command. The length of a single episode is 60, 80 and 100 for the *relocate* task, *place inside* task and *pour* task, respectively. We use PPO [66] to optimize the state-based policy. We set the learning rate and batch size to $1e-5$ and 256, respectively. The RL training takes around 30 hours on a single V100 GPU and 32 CPUs for each video separately. Our visual policy only requires robot proprioceptive states (the left part of Table I) and point clouds as inputs. To train the visual policy, we rollout 500 successful trajectories from the state-based policy for each video, where trajectories differ in initial object positions, rotations and target positions. During rollouts, we render 3D scene point clouds from three depth cameras surrounding the table in the simulation platform. We train the visual policy with Adam optimizer using a learning rate of $1e-5$ and a batch size of 64. It takes 8 hours on 4 A100 GPUs for our visual policy trained from 5 videos.

B. Evaluation of the State-based Policy on the Relocate Task

We adopt the *relocate* task to evaluate the state-based policy. Specifically, we use one DexYCB video for each of the five object categories and train a state-based policy for each video separately. The initial object poses of the videos are illustrated in the first row of Figure 4.

1) *Ablation Studies:* We first perform ablations to validate the importance of our hand rewards at the pre-grasp and the manipulation stages in state-based policy learning. Table II presents the averaged performance over the five videos

TABLE III: Comparison with state-of-the-art methods on the *relocate* task for state-based policies. We optimize a state-based policy using a single human video for each object (S6, S7), while previous methods usually need about one hundred human videos for each object (S2-S4). * indicates that we re-train the method from [23] with 20 DexYCB videos for each object.

Methods	Training algorithms	Num. videos	Mustard bottle		Tomato can		Sugar box		Large clamp		Mug		Avg.	
			SR ₁₀	SR ₃										
S1 DexMV [23]	TRPO [69]	0	0.06	-	0.67	-	0.00	-	0.51	-	0.49	-	0.35	-
S2 DexMV [23]	SOIL [70]	97	0.33	-	0.98	-	0.67	-	0.89	-	0.71	-	0.72	-
S3 DexMV [23]	GAIL+ [71]	97	0.06	-	0.66	-	0.00	-	0.52	-	0.53	-	0.50	-
S4 DexMV [23]	DAPG [19]	97	0.93	-	1.00	-	0.00	-	1.00	-	1.00	-	0.79	-
S5 DexMV [23]*	DAPG [19]	20	1.00	0.63	1.00	0.56	0.09	0.00	0.08	0.00	0.02	0.00	0.44	0.24
S6 Ours / wo rot.	PPO [66]	1	0.75	0.03	0.74	0.65	0.38	0.08	0.39	0.03	0.98	0.03	0.65	0.16
S7 Ours	PPO [66]	1	1.00	1.00										

TABLE IV: Performance of separate visual policies for each object on the *relocate* task. The initial configurations in testing are derived from the first row of Figure 4 for each object. Our visual policies (V4-V6) only utilize one video in training. ‘‘Comp. PC’’ denotes complete point clouds sampled from object CAD models without occlusion.

Source Models	Comp. PC	Object states	Visual inputs	Num. Points	Noisy Points	Mustard bottle		Tomato can		Sugar box		Large clamp		Mug		Avg.	
						SR ₁₀	SR ₃										
V1 S4	✓	✓	✓	512	×	1.00	0.67	1.00	0.50	0.14	0.00	1.00	0.77	1.00	0.58	0.83	0.50
V2 S4	×	✓	✓	512	×	1.00	0.62	1.00	0.48	0.14	0.00	1.00	0.76	0.99	0.55	0.83	0.48
V3 S4	×	×	✓	512	×	0.98	0.55	1.00	0.46	0.14	0.00	1.00	0.76	0.99	0.54	0.82	0.46
V4 S7	×	×	✓	512	×	1.00	0.89	1.00	0.86	1.00	0.96	1.00	0.91	1.00	1.00	1.00	0.92
V5 S7	×	×	✓	2048	×	1.00	0.97	1.00	0.80	1.00	0.98	1.00	0.93	1.00	1.00	1.00	0.94
V6 S7	×	×	✓	2048	✓	0.97	0.77	0.97	0.57	1.00	0.88	1.00	0.89	1.00	1.00	0.99	0.82

for policies with different reward functions. The policy in R1 uses the proposed hand rewards (*i.e.*, Equation 3) in the manipulation stage but follows the previous reward function [23], [28], [19] in the pre-grasp stage which is to minimize the distance between the robot hand and the object. It achieves poor performance due to the lack of guidance from human hand trajectory to approach the object. As shown in the first column of Figure 5, the policy is difficult to arrive at a plausible pre-grasp configuration to stably lift the object. The policy in R2 employs the proposed reward function in the pre-grasping stage (Equation 2) but follows PGDM [27] (*i.e.*, the second and forth terms in Equation 3) in the object manipulation stage. The reward function in PGDM constrains the object motions to be close to the reference trajectory but does not add any constraints on the hand motions, which results in unnatural robot hand actions as shown in the second column of Figure 5. Our proposed policy in R3 utilizes hand rewards in both stages, which outperforms R1 and R2 on all the metrics and produces robust and realistic grasps as shown in the last column of Figure 5.

2) *State-of-the-art comparison*: Table III presents the quantitative comparison of our state-based policy and state-of-the-art models [23]. S1 to S4 denote four model variants reported in [23]. As their training data is not released, we re-train their best model DAPG [19] (S4) using DexYCB videos and report the results in S5 for more fair comparison. We can see that the performance drops significantly for some objects, *i.e.*, *large clamp* and *mug*. This indicates that their method requires sufficient amount of videos to learn the manipulation of objects with complex shapes. Our proposed

policy in S7 significantly outperforms the previous methods despite only using one training video per object. Though S4 also performs well for *mustard bottle*, *tomato soup can*, *large clamp* and *mug*, it easily knocks down thin objects (*e.g.*, *sugar box*) when the robot approaches the object and achieves poor performance. Our hand reward addresses this problem by mimicking the human pre-grasping trajectory. S6 is a variant of our model without rotation augmentation in training. The inferior performance of S6 to our final model S7 demonstrates the importance of augmentation to help improve the robustness of trained policies.

C. Evaluation of the Visual Policy on the Relocate Task

Here, we evaluate our proposed visual policy on the *relocate* task and present a detailed experimental analysis.

1) *Learning from a single video per object*: We first explore training separate visual policies for each object with only one video as in the previous section IV-B. During testing, we use the same object configurations as in the section IV-B, which are derived from object poses in the first row of Figure 4 by randomly changing the initial object position and rotation around z-axis for each testing episodes. The results are presented in Table IV. From V1 to V3, we rollout trajectories from the S4 models in Table III ¹ to train the visual policy. V1 has the same assumption as [28] which assumes known object states and complete object point clouds. V2 removes the dependency on complete point clouds but still requires object states. V3 further relaxes the assumption and only uses robot states together with scene point clouds. We

¹We use S4 models available at released codes of DexMV [23].

TABLE V: Performance of separate policies for each object on the *relocate* task. The initial configurations in testing are derived from all three rows in Figure 4. We compare our visual policies using different number of training videos. “Mb.”, “Tc.”, “Sb.” and “Lc.” denote *mustard bottle*, *tomato can*, *sugar box* and *large clamp* respectively.

Num. videos	Mb.		Tc.		Sb.		Lc.		Mug		Avg.		
	SR ₁₀	SR ₃											
S4	97	0.46	0.28	0.59	0.35	0.11	0.00	0.63	0.31	0.65	0.62	0.49	0.31
V5	1	0.33	0.32	0.41	0.25	0.33	0.32	0.43	0.31	0.58	0.57	0.42	0.35
V7	2	0.65	0.42	0.66	0.60	0.66	0.62	0.67	0.64	0.91	0.85	0.71	0.63
V8	3	0.96	0.66	0.95	0.82	0.89	0.63	0.98	0.92	0.98	0.97	0.95	0.80

TABLE VI: Performance of unified visual policies for all objects on the *relocate* task. The initial configurations in testing are derived from all three rows in Figure 4. We compare point cloud representations with different coordinate systems where “wo.”, “ta.” and “ha.” represent world, target and robot hand. “Mb.”, “Tc.”, “Sb.” and “Lc.” denote *mustard bottle*, *tomato can*, *sugar box* and *large clamp* respectively.

Coord. sys	Mb.		Tc.		Sb.		Lc.		Mug		Avg.		
	wo.ta.ha.	SR ₁₀	SR ₃										
V9	✓ × ×	0.77	0.32	0.73	0.44	0.80	0.29	0.87	0.40	0.79	0.58	0.79	0.41
V10	✓ ✓ ×	0.91	0.84	0.94	0.92	0.99	0.97	0.96	0.93	0.92	0.92	0.94	0.92
V11	✓ ✓ ✓	0.94	0.86	0.99	0.98	0.98	0.93	0.99	0.97	0.96	0.95	0.97	0.94

can see that performance decreases when using no privileged object information (*i.e.*, object states and complete object point clouds). From V4 to V6, we train the visual policy using rollouts from our state-based policies S7. Benefiting from high-quality trajectories generated by S7, our visual policy V4 can outperform V1 to V3 by a large margin without privileged information. To investigate how the density of point clouds affect the visual policy, we sample 2048 points in V5 at each timestep. This marginally improves the performance compared to V4. In V6 we evaluate the robustness of our visual policy by adding Gaussian noise with $\sigma=3\text{cm}$ to 3D point clouds during training and testing. Our visual policy still functions reasonably under noisy point clouds observations.

2) *Learning from multiple videos per object*: We next introduce a more challenging testing scenario where we evaluate policies under three different initial object configurations for each object as shown in Figure 4. For example, the mustard bottle does not necessarily stand on the table, but can lie in different ways. Table V presents the results of different models. The state-based policy S4 [23] in Table III though employs privilege object information and multiple videos per object in training, still generalizes poorly to different initial object poses. Our visual policy V5 in Table IV also suffers in this challenging testing scenario due to the insufficient training videos. From V7 to V8, we gradually increase the number of training videos with diverse initial object configurations and demonstrate significant increase in performance.

3) *Learning a unified multi-object visual policy from multiple videos*: Finally, we train a single policy for all objects and configurations and report its performance in Table VI. We test the policy under three initial configurations for each

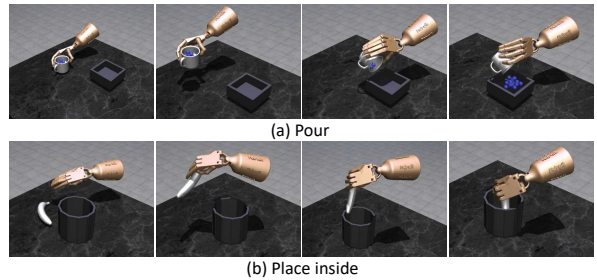


Fig. 6: Qualitative illustration of the performance of our visual policies on *pour* (a) and *place inside* (b) tasks.

TABLE VII: Comparison with state-of-the-art methods on the *pour* and the *place inside* tasks for our policy models. Our approach uses a single human video for each task, while previous methods need more than 91 human videos.

Methods	Training algorithms	Num. videos	Pour success rate	Place inside success rate
S1	DexMV [23]	TRPO [69]	0 / 0	0.01
S2	DexMV [23]	SOIL [70]	101 / 91	0.04
S3	DexMV [23]	GAIL+ [71]	101 / 91	0.03
S4	DexMV [23]	DAPG [19]	101 / 91	0.27
S7	Ours	PPO [66]	1 / 1	0.97
V5	Ours	Behavior cloning	1 / 1	0.97

object as the above paragraph. The visual policy V9 has the same architecture as the policy V8 in Table V, which uses 3D point clouds represented in the world coordinate frame. By comparing V9 and V8, we can see that learning a unified model is more challenging than training policies for each object separately. Therefore, we improve the point cloud representations in the visual policy. In V10, we transform the 3D point clouds to the target coordinate system. As result, the model becomes more aware of its target and improves the performance significantly, *i.e.*, 79% to 94% under SR₁₀. To further incorporate fine-grained hand-object interaction features, we additionally transform 3D points into six hand joint coordinate systems in V11 (*i.e.*, five finger tips and the hand wrist). Benefiting from extracting rich hand-object interaction features, our final model achieves an average success rate of 97% under SR₁₀ for the five objects under the challenging test scenario with three different configurations.

D. Evaluation of our policy on Pour and Place inside Tasks

We further evaluate our approach on the *pour* and *place inside* tasks. Table VII shows the quantitative results. Rows S1 to S4 are state-based policies reported in [23] where they use 91 videos and 101 videos for pour and place inside tasks respectively. While we only adopt one video in training, our state-based policy S7 achieves 97% and 68% success rates on the two tasks respectively, significantly outperforming 27% and 31% success rates using their best models. Benefiting from high-quality trajectories generated by our state-based policies, our visual policies V5 also achieve good performance on these two tasks. Figure 6 illustrates qualitative examples from our visual policy for these two tasks.

V. CONCLUSION

We introduce ViViDex, a new framework to learn vision-based dexterous manipulation from human videos. To this end, we first extract reference hand and object trajectories from human videos and train state-based policies via RL to generate diverse physically plausible trajectories as the training data for the vision-based policy. Then, the visual policy takes robot proprioceptive states and 3D point clouds as inputs and further transforms 3D point clouds into different coordinate systems to achieve better performance. We conduct extensive ablations experiments to validate the effectiveness of our ViViDex system. We show that our visual policies can outperform state-of-the-art accuracy by a great margin on three dexterous manipulation tasks. Future work aims at leveraging internet videos for acquiring more general dexterous manipulation skills and investigating advanced 3D pose estimators.

Acknowledgement: This work was granted access to the HPC resources of IDRIS under the allocation AD011013147 made by GENCI. It was funded in part by the French government under management of Agence Nationale de la Recherche as part of the “Investissements d’avenir” program, reference ANR19-P3IA-0001 (PRAIRIE 3IA Institute) and the ANR project VideoPredict (ANR-21-FA11-0002-01).

REFERENCES

- [1] S. James, Z. Ma, D. R. Arrojo, and A. J. Davison, “RLbench: The robot learning benchmark & learning environment,” *RAL*, 2020.
- [2] P.-L. Guhur, S. Chen, R. G. Pinel, M. Tapaswi *et al.*, “Instruction-driven history-aware policies for robotic manipulations,” in *CoRL*, 2023.
- [3] D. Driess, F. Xia, M. S. Sajjadi, C. Lynch, A. Chowdhery *et al.*, “Palm-e: An embodied multimodal language model,” in *ICML*, 2023.
- [4] S. Chen, R. Garcia, C. Schmid, and I. Laptev, “Polarnet: 3d point clouds for language-guided robotic manipulation,” in *CoRL*, 2023.
- [5] M. Liu, X. Li, Z. Ling, Y. Li *et al.*, “Frame Mining: a free lunch for learning robotic manipulation from 3D point clouds,” in *CoRL*, 2022.
- [6] C. Chi, S. Feng, Y. Du, Z. Xu, E. Cousineau *et al.*, “Diffusion policy: Visuomotor policy learning via action diffusion,” in *RSS*, 2023.
- [7] M. T. Mason, “Toward robotic manipulation,” *Annual Review of Control, Robotics, and Autonomous Systems*, 2018.
- [8] Y. LeCun, Y. Bengio, and G. Hinton, “Deep learning,” *Nature*, 2015.
- [9] L. P. Kaelbling *et al.*, “Reinforcement learning: A survey,” *Journal of artificial intelligence research*, 1996.
- [10] R. S. Sutton *et al.*, *Reinforcement learning: An introduction*, 2018.
- [11] H. Qi, A. Kumar, R. Calandra, Y. Ma, and J. Malik, “In-hand object rotation via rapid motor adaptation,” in *CoRL*, 2022.
- [12] Z.-H. Yin, B. Huang, Y. Qin, Q. Chen, and X. Wang, “Rotating without seeing: Towards in-hand dexterity through touch,” in *RSS*, 2023.
- [13] H. Qi, B. Yi, S. Suresh, M. Lambeta, Y. Ma, R. Calandra, and J. Malik, “General in-hand object rotation with vision and touch,” in *CoRL*, 2023.
- [14] I. Akkaya, M. Andrychowicz, M. Chociej, M. Litwin *et al.*, “Solving rubik’s cube with a robot hand,” *arXiv*, 2019.
- [15] H. Xu, Y. Luo, S. Wang, T. Darrell, and R. Calandra, “Towards learning to play piano with dexterous hands and touch,” in *IROS*, 2022.
- [16] K. Zakka, P. Wu, L. Smith, N. Gileadi *et al.*, “Robopianist: Dexterous piano playing with deep reinforcement learning,” in *CoRL*, 2023.
- [17] S. J. Russell and P. Norvig, *Artificial intelligence a modern approach*. London, 2010.
- [18] J. Merel, Y. Tassa *et al.*, “Learning human behaviors from motion capture by adversarial imitation,” *arXiv*, 2017.
- [19] A. Rajeswaran *et al.*, “Learning complex dexterous manipulation with deep reinforcement learning and demonstrations,” in *RSS*, 2018.
- [20] Y. Qin, W. Yang, B. Huang *et al.*, “Anyteleop: A general vision-based dexterous robot arm-hand teleoperation system,” in *RSS*, 2023.
- [21] S. P. Arunachalam *et al.*, “Dexterous imitation made easy: A learning-based framework for efficient dexterous manipulation,” in *ICRA*, 2023.
- [22] S. P. Arunachalam, I. Güzey, S. Chintala, and L. Pinto, “Holo-Dex: Teaching dexterity with immersive mixed reality,” in *ICRA*, 2023.
- [23] Y. Qin, Y.-H. Wu, S. Liu, H. Jiang *et al.*, “DexMV: Imitation learning for dexterous manipulation from human videos,” in *ECCV*, 2022.
- [24] P. Mandikal and K. Grauman, “DexVIP: Learning dexterous grasping with human hand pose priors from video,” in *CoRL*, 2022.
- [25] Q. Liu *et al.*, “DexRepNet: Learning dexterous robotic grasping network with geometric and spatial hand-object representations,” in *IROS*, 2023.
- [26] K. Shaw, S. Bahl, and D. Pathak, “VideoDex: Learning dexterity from internet videos,” in *CoRL*, 2022.
- [27] S. Dasari, A. Gupta, and V. Kumar, “Learning dexterous manipulation from exemplar object trajectories and pre-grasps,” in *ICRA*, 2023.
- [28] Y.-H. Wu, J. Wang, and X. Wang, “Learning generalizable dexterous manipulation from human grasp affordance,” in *CoRL*, 2022.
- [29] A. Bicchi and V. Kumar, “Robotic grasping and contact: A review,” in *ICRA*, 2000.
- [30] L. Han and J. C. Trinkle, “Dextrous manipulation by rolling and finger gaiting,” in *ICRA*, 1998.
- [31] D. Rus, “In-hand dexterous manipulation of piecewise-smooth 3D objects,” *IJRR*, 1999.
- [32] I. Mordatch, Z. Popović, and E. Todorov, “Contact-invariant optimization for hand manipulation,” in *SIGGRAPH*, 2012.
- [33] A. Wu *et al.*, “Learning diverse and physically feasible dexterous grasps with generative model and bilevel optimization,” *arXiv*, 2022.
- [34] S. Nair, A. Rajeswaran, V. Kumar, C. Finn, and A. Gupta, “R3M: A universal visual representation for robot manipulation,” in *CoRL*, 2022.
- [35] Y. Xu, W. Wan, J. Zhang, H. Liu, Z. Shan, H. Shen, R. Wang *et al.*, “UniDexGrasp: Universal robotic dexterous grasping via learning diverse proposal generation and goal-conditioned policy,” in *CVPR*, 2023.
- [36] T. Chen, J. Xu, and P. Agrawal, “A system for general in-hand object re-orientation,” in *CoRL*, 2021.
- [37] C. Bao, H. Xu, Y. Qin *et al.*, “DexArt: Benchmarking generalizable dexterous manipulation with articulated objects,” in *CVPR*, 2023.
- [38] W. Wan, H. Geng, Y. Liu, Z. Shan *et al.*, “UniDexGrasp++: Improving dexterous grasping policy learning via geometry-aware curriculum and iterative generalist-specialist learning,” in *ICCV*, 2023.
- [39] A. Nagabandi, K. Konolige, S. Levine, and V. Kumar, “Deep dynamics models for learning dexterous manipulation,” in *CoRL*, 2020.
- [40] N. Hansen, Y. Lin, H. Su *et al.*, “MoDem: Accelerating visual model-based reinforcement learning with demonstrations,” in *ICLR*, 2023.
- [41] H. Jiang, S. Liu, J. Wang, and X. Wang, “Hand-object contact consistency reasoning for human grasps generation,” in *ICCV*, 2021.
- [42] R. Rubinfeld, “The cross-entropy method for combinatorial and continuous optimization,” 1999.
- [43] Y.-W. Chao, W. Yang, Y. Xiang, P. Molchanov *et al.*, “DexYCB: A benchmark for capturing hand grasping of objects,” in *CVPR*, 2021.
- [44] Y. Liu, Y. Liu, C. Jiang, K. Lyu *et al.*, “HOI4D: A 4D egocentric dataset for category-level human-object interaction,” in *CVPR*, 2022.
- [45] Y. Hasson, G. Varol, D. Tzionas, I. Kalevtykh *et al.*, “Learning joint reconstruction of hands and manipulated objects,” in *CVPR*, 2019.
- [46] Z. Chen, S. Chen, C. Schmid *et al.*, “gSDF: Geometry-Driven signed distance functions for 3D hand-object reconstruction,” in *CVPR*, 2023.
- [47] Y. Ye, A. Gupta, and S. Tulsiani, “What’s in your hands? 3D reconstruction of generic objects in hands,” in *CVPR*, 2022.
- [48] L. Smith, N. Dhawan, M. Zhang *et al.*, “Avid: Learning multi-stage tasks via pixel-level translation of human videos,” in *RSS*, 2020.
- [49] K. Zakka, A. Zeng, P. Florence, J. Tompson, J. Bohg *et al.*, “Xirl: Cross-embodiment inverse reinforcement learning,” in *CoRL*, 2021.
- [50] F. Ebert, Y. Yang *et al.*, “Bridge data: Boosting generalization of robotic skills with cross-domain datasets,” in *RSS*, 2022.
- [51] K. Schmeckpeper *et al.*, “Reinforcement learning with videos: Combining offline observations with interaction,” in *CoRL*, 2020.
- [52] L. Shao, T. Migimatsu *et al.*, “Concept2robot: Learning manipulation concepts from instructions and human demonstrations,” in *RSS*, 2020.
- [53] T. Xiao, I. Radosavovic, T. Darrell, and J. Malik, “Masked visual pre-training for motor control,” *arXiv*, 2022.
- [54] I. Radosavovic, T. Xiao, S. James, P. Abbeel, J. Malik *et al.*, “Real-world robot learning with masked visual pre-training,” in *CoRL*, 2023.
- [55] Y. Ze, Y. Liu, R. Shi, J. Qin, Z. Yuan, J. Wang, and H. Xu, “H-InDex: visual reinforcement learning with hand-informed representations for dexterous manipulation,” in *NeurIPS*, 2023.
- [56] K. Grauman, A. Westbury, E. Byrne *et al.*, “Ego4D: Around the world in 3,000 hours of egocentric video,” in *CVPR*, 2022.
- [57] A. S. Chen, S. Nair, and C. Finn, “Learning generalizable robotic reward functions from” in-the-wild” human videos,” in *RSS*, 2021.
- [58] M. Alakuijala, G. Dulac-Arnold *et al.*, “Learning reward functions for robotic manipulation by observing humans,” in *ICRA*, 2023.
- [59] E. Chane-Sane, C. Schmid, and I. Laptev, “Learning video-conditioned policies for unseen manipulation tasks,” in *ICRA*, 2023.

- [60] H. Xiong, Q. Li, Y.-C. Chen *et al.*, “Learning by watching: Physical imitation of manipulation skills from human videos,” in *IROS*, 2021.
- [61] P. Mandikal and K. Grauman, “Learning dexterous grasping with object-centric visual affordances,” in *ICRA*, 2021.
- [62] J. Romero, D. Tzionas, and M. J. Black, “Embodied Hands: Modeling and capturing hands and bodies together,” *TOG*, 2017.
- [63] A. Handa, K. Van Wyk, W. Yang *et al.*, “DexPilot: Vision-based teleoperation of dexterous robotic hand-arm system,” in *ICRA*, 2020.
- [64] D. Antotsiou, G. Garcia-Hernando *et al.*, “Task-oriented hand motion retargeting for dexterous manipulation imitation,” in *ECCV*, 2018.
- [65] G. J. Steven, “The nlopt nonlinear-optimization package,” 2019.
- [66] J. Schulman, F. Wolski, P. Dhariwal, A. Radford *et al.*, “Proximal policy optimization algorithms,” *arXiv*, 2017.
- [67] C. R. Qi, H. Su, K. Mo, and L. J. Guibas, “PointNet: Deep learning on point sets for 3D classification and segmentation,” in *CVPR*, 2017.
- [68] E. Todorov, T. Erez, and Y. Tassa, “MuJoCo: A physics engine for model-based control,” in *IROS*, 2012.
- [69] J. Schulman *et al.*, “Trust region policy optimization,” in *ICML*, 2015.
- [70] I. Radosavovic, X. Wang, L. Pinto, and J. Malik, “State-only imitation learning for dexterous manipulation,” in *IROS*, 2021.
- [71] B. Kang, Z. Jie, and J. Feng, “Policy optimization with demonstrations,” in *ICML*, 2018.